Electrochimica Acta 89 (2013) 814–822

Contents lists available at SciVerse ScienceDirect

Electrochimica Acta

journal homepage: www.elsevier.com/locate/electacta

Characterization of film properties on the Ni—Cr—Mo Alloy C-2000

Xiangrong Zhang[a], Dmitrij Zagidulin[a], David W. Shoesmith[a,b,*]

[a] Department of Chemistry, University of Western Ontario, London, Ontario N6A 5B7, Canada
[b] Surface Science Western, University of Western Ontario, London, Ontario N6G 0J3, Canada

ARTICLE INFO

Article history:
Received 3 October 2012
Received in revised form 8 November 2012
Accepted 9 November 2012
Available online 19 November 2012

Keywords:
Passive film
Ni—Cr—Mo alloys
Alloy C-2000
XPS
ToF-SIMS

ABSTRACT

The passive and transpassive film properties grown at various potentials on a Ni—Cr—Mo alloy, Alloy C-2000 (Ni—23Cr—16Mo—1.6Cu), were investigated by surface-sensitive techniques such as Angle-Resolved X-ray Photoelectron Spectroscopy (AR-XPS), Time-of-Flight Secondary Ion Mass Spectrometry (ToF-SIMS) and SEM. The presence of a layered structure in the passive film has been demonstrated, with the outermost surface being enriched in Cu (or Cu oxide) and Mo oxide, the intermediate region dominated by Cr/Ni hydroxides, and the inner region comprising Cr/Ni oxide.

As the potential increases from −0.4 to 0.6 V (vs. Ag/AgCl in saturated KCl), the film thickness increases, and the relative Cr content of the film increases while that of Ni decreases. The passive film (0 V) has a relatively thicker inner oxide layer and higher Cr_2O_3 content in the inner layer, compared to the near-passive film (−0.4 V). In the transpassive region (0.6 V), the anodic oxidation of Cr(III) to Cr(VI) in the barrier layer of the film and its subsequent dissolution leads to the loss of the Cr_2O_3-rich inner layer and the destruction of passivity. Destruction of the barrier layer proceeds non-uniformly on the alloy surface.

1. Introduction

It is well known that Ni—Cr—Mo alloys exhibit exceptional corrosion resistance under extreme exposure conditions. These alloys are widely used by chemical processing industries, in the areas of energy, health and environmental, oil, and gas and pharmaceuticals. Their high corrosion resistance is generally attributed to their elemental composition and the passive behavior it induces; the combination of high Cr and Mo contents leading to the formation of a Cr-dominated passive oxide film [1–5]. Since the properties of passive films control overall corrosion behavior, a wide array of in situ and ex situ analytical techniques [1,3,6–10] has been employed to assess the passive behavior and passive film properties on Ni—Cr—Mo alloys. Additionally, the high percentage of $\sum 3$ grain boundaries limits the initiation of localized corrosion at these locations [11] and the high Mo content limits propagation and promotes rapid repassivation if initiation of localized sites does occur [12].

Lloyd et al. [1–3] determined the film composition and thickness, and the effect of the alloying elements, Cr, Mo and W, on the composition and thickness of the passive film on a number of Ni—Cr—Mo (W) alloys in acidic solutions. The oxide film consists of a Mo, Cr, and Ni oxide, with Cr present as Cr(III) and Mo present in several oxidation states. The film was found to be only a few nanometers thick (<5 nm), and the thickness increased with increasing potential in the passive region. Time-of-Flight Secondary Ion Mass Spectrometry (ToF-SIMS) and X-ray Photoelectron Spectroscopy (XPS) showed that the high-Cr alloys were able to build thicker oxides with a layered structure consisting of an inner Cr—Ni oxide layer and an outer Mo/W oxide when anodically oxidized in 1.0 M NaCl + 0.1 M H_2SO_4 solution (pH 1). The presence of Mo and W in the outer regions of the oxide is thought to suppress passive dissolution at high potentials, when Cr(VI) release appears to start. A similar layered oxide was observed to form on Alloy-22 (Ni—22Cr—13Mo—3W) in extremely saline (5 M NaCl) neutral solutions [13], over the potential range −0.4 V to 0.2 V. A Cr(III) oxide barrier layer was shown to grow and thicken with increasing potential, again accompanied by the segregation of Mo, and to a lesser degree W, to the outer regions of the film.

The oxide film properties have also been characterized by electrochemical impedance spectroscopy (EIS) [6,8,14]. MacDonald et al. [8] characterized the oxide properties on Alloy-22 over the potential range from −0.2 to 0.7 V. The polarization resistance (R_p), dominated by the barrier layer resistance, measured in hot, slightly acidic solution (pH 3, saturated NaCl, 80 °C), initially increased with applied potential within the passive range achieving values $>10^5\ \Omega\ cm^2$ consistent with passivity. At a sufficiently high potential ($E > 0.2$ V), close to the initiation of the transpassive state, R_p begins to decrease with increasing potential. The film exhibited n-type semiconducting properties in the passive region (<0.4 V) with

* Corresponding author.
E-mail address: dwshoesm@uwo.ca (D.W. Shoesmith).

0013-4686/$ – see front matter © 2012 Elsevier Ltd. All rights reserved.
http://dx.doi.org/10.1016/j.electacta.2012.11.029

a transition to p-type behavior as the oxide thinned and cations were oxidatively ejected from the barrier layer in the transpassive region [14].

Recently, Jakupi et al. [6] characterized the oxide film properties on Alloy-22 in near neutral pH, 5 M NaCl solutions, at 30 °C. A similar variation in film resistance with applied potential was observed, the impedance properties being divided into three applied potential ranges. More recently, the evolution of surface composition in these three regions has been determined by XPS [13]. Over the potential range −0.6 V to ∼−0.3 V, the film resistance increases with potential accompanied by an increase in Cr(III) content indicating the formation of a protective barrier layer. Both the film resistance and the Cr(III) content of the oxide increase to their maximum values in the potential range −0.3 V to ∼0.3 V accompanied by a decrease in the relative concentration of Ni in the film [13]. Within this range the Mo content of the film (as Mo(II), Mo(IV), Mo(VI) and non-stoichiometric Mo_4O_{11}) does not vary significantly with potential [13]. For potentials >0.3 V, both the film resistance and the Cr(III) content decrease accompanied by significant increases in $Cr(OH)_3$, Mo(VI) and W(VI), indicating the injection of cation defects into the Cr(III) oxide-dominated barrier layer in the early stages of transpassivity.

Crevice corrosion experiments conducted under galvanostatic conditions showed that a potential >0.2 V was required to initiate and stabilize active crevice corrosion at 120 °C in 5 M NaCl. This apparent threshold for initiation is consistent with a susceptibility to crevice corrosion only when defect injection into the Cr(III) oxide barrier layer occurs, as identified by XPS and impedance measurements.

The susceptibility of Ni—Cr alloys to crevice corrosion is clearly dependent on the composition of the alloy [15–17], although the critical compositional balance remains unelucidated. In an attempt to clarify the key compositional features we have been studying a range of alloys. In this paper we describe our studies on the oxide composition on Alloy C-2000 (Ni—23Cr—16Mo—1.6Cu) as a function of applied potential using Angle-Resolved X-ray Photoelectron Spectroscopy (AR-XPS) and ToF-SIMS.

2. Experimental

2.1. Materials and electrode preparation

Cylindrical specimens were cut from plate material supplied by Haynes International, Kokomo, Indiana (USA), with a diameter of 1 cm and a height of 0.5–1 cm. The cylinders were drilled at one end to allow electrical connection to a threaded rod of the same material. Prior to each experiment, the specimen surface (surface area of 0.785 cm^2) was wet-polished with a series of SiC papers up to 1200 grit, and then polished successively with 5.0, 0.3, and 0.05 μm alumina powder suspensions. Specimens were then swabbed with cotton under running water to reduce the chances of staining, and finally rinsed with large amounts of Type 1 water, obtained from a Milli-Q Academic A-10 system. Specimens were immersed first in acetone and then in Type 1 water and ultrasonicated for 10 min to remove any attached polishing residue, rinsed again with large amounts of Type 1 water, and immediately placed in the electrochemical cell to minimize air oxidation.

2.2. Electrochemical film growth

A standard three-electrode, glass electrochemical cell housed in a grounded Faraday cage was used. The cell contains a working electrode (WE), a pure platinum (99.95% purity) counter electrode (CE), and an in-house fabricated saturated silver/silver chloride (Ag/AgCl) reference electrode (RE) (199 mV vs. SHE at 25 °C). Freshly prepared 5 M NaCl solutions were used as the electrolyte. The solutions were prepared from reagent grade NaCl and Type 1 water. Prior to starting each experiment, the electrolyte solution was purged for at least 1 h with UHP argon (Praxair) and purging continued throughout the experiment.

A Solartron 1284 multistat was used to apply a constant potential to the electrode, half-immersed in a stirred electrolyte. A period of 60 min of cathodic cleaning at −1.0 V was required to guarantee a reproducible surface. Subsequently, a film formation potential was applied for 44 h to grow an oxide film, and Corrware software (Scribner Associates Inc.) was used to record the data. The potentials investigated were −0.4, 0, and 0.6 V to represent near-passive, passive and transpassive regions, respectively [1]. Experiments were performed at room temperature (22 ± 2 °C). The pH of the solutions was adjusted to 7.0 ± 0.2 with HCl and NaOH solutions.

After film-growth, the specimen was immediately removed from the cell, rinsed and ultrasonicated for 2 min in Type 1 water to remove any electrolyte left on the specimen surface. The specimen surface was then dried in a stream of argon gas, placed in a small tin box and stored in a desiccator. Subsequently, the specimen was analyzed using SEM, XPS and ToF-SIMS.

2.3 Surface analyses

SEM images were obtained on a Hitachi S-4500 field emission SEM equipped with an EDAX™ EDX system at Surface Science Western (SSW). All AR-XPS analyses were carried out with a Kratos Axis Ultra spectrometer at SSW using a monochromatic Al Kα (1486.6 eV) source. The instrument work function was calibrated to give an Au 4f7/2 metallic gold binding energy of 83.95 eV. The spectrometer dispersion was adjusted to give a binding energy of 932.63 eV for metallic Cu 2p3/2. The Kratos charge neutralizer system was used for all analyses. The apparent shifts of the spectra were calibrated using the C 1s peak set to 284.8 eV. High-resolution spectra were obtained using a 20 eV pass energy, whereas survey spectra were recorded using a 160 eV pass energy with an analysis area of ∼300 μm × 700 μm. Two photoelectron take-off angles (measured from the sample surface), 30° and 90°, were used to analyze the oxide film on Alloy C-2000. By comparison of the information obtained at a grazing take-off angle (30°) to that at an angle close to the surface normal (90°), information on the variation of composition with depth can be obtained.

An ION-ToF Time-of-Flight Secondary Ion Mass Spectrometer (ToF-SIMS IV) was used to obtain the ToF-SIMS depth profiles and cross-sectional images for sputtered specimens. A 1 kV Cs^+ ion beam was used to sputter an area of 200 μm × 200 μm on the specimen and negative secondary ions were collected from a 100 μm × 100 μm area within the sputter crater using a 25 kV monoisotopic Bi_3^+ primary ion beam. A smaller analysis area was used within the sputter crater to avoid edge effects. Each ToF-SIMS mass spectrum was calibrated using the exact mass values of at least 3 known species in the spectrum collected during profiling.

3. Results

3.1. Electrochemical film growth

Fig. 1 shows log–log plots of current density transients recorded at the three potentials (−0.4, 0, and 0.6 V) in deoxygenated neutral 5 M NaCl at room temperature. These potentials cover the range from incomplete passivation (−0.4 V) to transpassivity (0.6 V) [1]. For times $\leq 10^2$ s the current is almost independent on time. This can be attributed to the change in composition of the cathodically reduced air-formed film remaining after the cathodic pretreatment. For $t \geq 3 \times 10^2$ s, the transients recorded at −0.4 V and 0 V

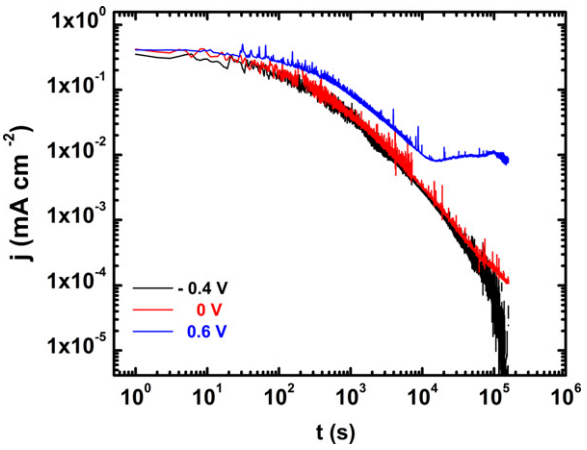

Fig. 1. Log current density (j)–log time (t) plots recorded on Alloy C-2000 at three potentials (−0.4, 0, and 0.6 V) in deoxygenated neutral 5 M NaCl at room temperature.

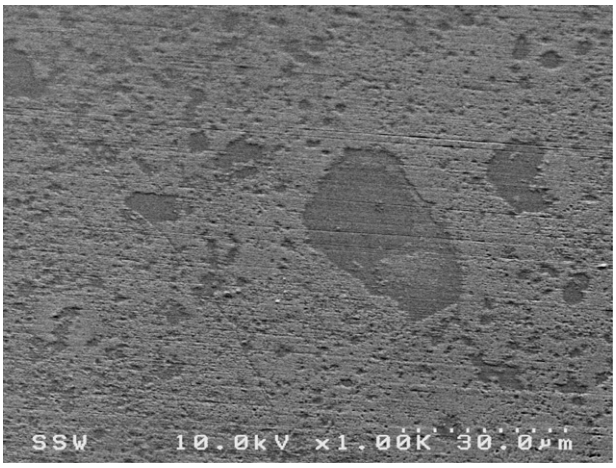

Fig. 2. SEM micrograph of the surface of Alloy C-2000 after polarization at 0.6 V (pH 7) for 44 h.

show the decay expected for oxide film growth with the net current at −0.4 V becoming negative after 36 h. The current densities observed at the end of the film growth period are in the range of 100 nA cm^{-2}, confirming the establishment of passivity. The current density recorded at 0.6 V initially decreases due to film growth before eventually increasing slightly after 4 h, indicating the onset of transpassivity. This is consistent with the transpassive oxidation of Cr(III) in the oxide film to the more soluble Cr(VI), and the conversion of Mo from low to high oxidation states [2]. The slight decrease in current density after 27 h suggests that thickening of the transpassive oxide limits the oxidation of the substrate alloy.

3.2. SEM and ToF-SIMS imaging

SEM micrographs show that, except after polarization at 0.6 V, the oxide-covered electrode surfaces are featureless and not shown. Fig. 2 shows the alloy surface after polarization at 0.6 V for 44 h is not uniformly oxide-covered as observed at the lower potentials: some areas are covered by a dark gray product, suggesting transpassive oxidation is uneven.

ToF-SIMS images of the surfaces oxidized at 0 V and 0.6 V, Fig. 3, confirm the uneven nature of the transpassive oxidation at 0.6 V. At this potential the various species are inhomogeneously distributed

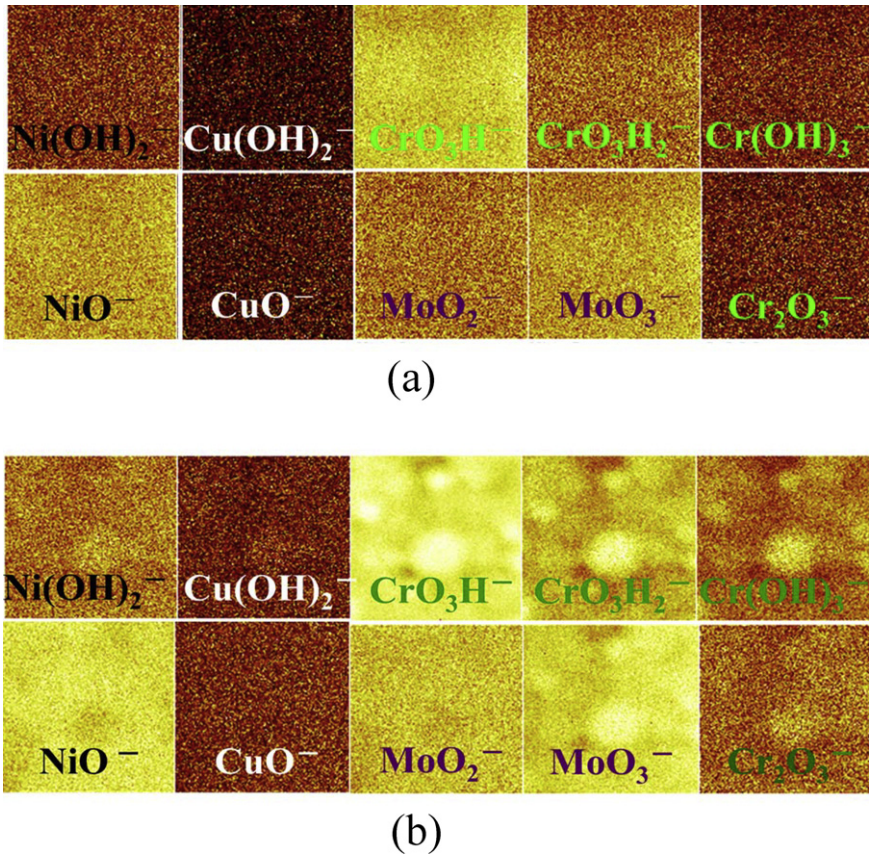

Fig. 3. ToF-SIMS images (top view, 100 μm × 100 μm) of the surface of Alloy C-2000 after polarization at (a) 0 V and (b) 0.6 V (pH 7). The lighter areas indicate a higher content of the species indicated. (For interpretation of the references to color in this figure legend, the reader is referred to the web version of this article.)

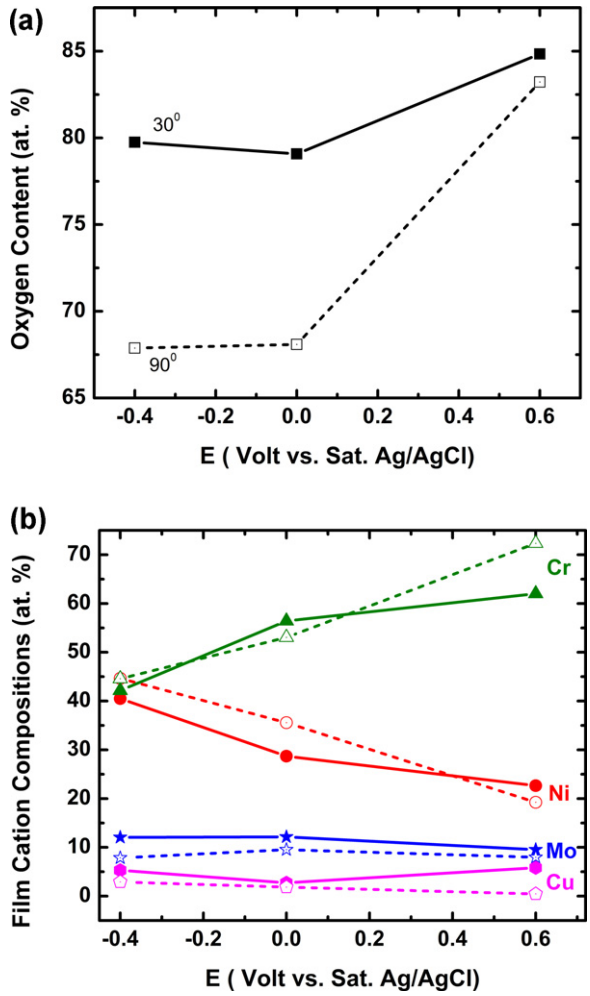

Fig. 4. Oxygen content (a) and film cation compositions (b) determined from the survey spectra recorded on Alloy C-2000 after polarization at −0.4 V, 0 V and 0.6 V (pH 7, 44 h) at take-off angles of 30° (solid line) and 90° (dashed line). The latter is corrected for contributions from the metallic substrate.

on a scale which matches the dimensions of the dark gray areas in the SEM image. Chromium hydroxide is enriched in the dark gray areas in the SEM image, accompanied by enrichment in MoO_3^- at the expense of MoO_2^-. Also, although less obvious, Ni and Cu hydroxides are enriched at the expense of the corresponding oxides. By contrast, all the species detected in the film grown at 0 V are uniformly distributed on the surface.

This non-homogeneity in the distribution of species and the almost time-independent current density at 0.6 V, Fig. 1, indicate that transpassive oxidation tends to spread laterally across the surface. This suggests oxidation occurs at the edges of unconverted passive oxide and that the high oxidation states of Mo produced transpassively from a partially protective thicker transpassive film.

3.3 Angle-resolved XPS

Electrodes polarized at −0.4 V, 0 V and 0.6 V were analyzed by AR-XPS at take-off angles of 30° and 90°. Analyses performed at the take-off angle of 30° probe shallower depths than those recorded at an angle of 90°. Surface compositions determined from survey spectra recorded at the two angles are shown in Fig. 4. As expected, the O relative content of the surface is higher at 30° than at 90° at −0.4 V and 0 V, Fig. 4(a). At 0.6 V the O content measured at 90° is only marginally less than that at 30° consistent with an increase in film thickness after anodic oxidation at this transpassive potential. The cation composition of the oxide film, corrected for contributions from the metallic substrate (determined from high-resolution spectra), is determined by excluding the oxygen contribution in the spectral quantification, Fig. 4(b). The film was found to be composed of ~40–70% Cr, 20–45% Ni, 10–20% Mo and a detectable amount of Cu depending on the polarization potential. Comparison to the nominal composition of Alloy C-2000 shows a clear enrichment of Cr and depletion of Ni in the film, especially after polarization at 0.6 V in the transpassive region.

For both Cu and Mo, the content is higher at 30° than 90° for all three potentials, suggesting their enrichment in the outer regions of the film. However, the differences are small precluding any definite conclusions. A similar slightly more definite comparison suggests Ni, and possibly Cr, are enriched in the inner regions at the two lower potentials. At 0.6 V the Cr content is considerably lower and that of Ni slightly higher at 30° compared to 90°, consistent with the transpassive oxidation of Cr(III) to Cr(VI) in the barrier layer of the film and its subsequent dissolution. If confirmed this Cr/Mo segregation in the film is consistent with the results of Lloyd et al. obtained on Ni—Cr—Mo alloys in acidic sulphate solution [2].

High-resolution scans were recorded for the Ni 2p, Cr 2p, Mo 3d, Cu 2p, O 1s and C 1s peaks. Examples of the fitted O 1s, Ni 2p, Cr 2p and Mo 3d spectra, corrected using a Shirley background correction, are shown in Fig. 5, and the relative amounts of individual species in Fig. 6. The O 1s spectrum can be fitted with three component peaks (Fig. 5(a)): the peaks at 529–530 eV, 531–532 eV and ~533 eV are attributed to O^{2-} in the oxide, $OH^{\cdot\cdot}$ species or defective sites in the oxide, and adsorbed H_2O (or possibly O_2) [18], respectively. The relative amounts of O^{2-} and OH^- obtained by fitting the O 1s spectra at the three potentials are shown in Fig. 6(a). Large amounts of OH^- are found at all three potentials, but especially at 0.6 V. The presence of large amounts of OH^- is likely due to the prolonged cathodic pretreatment of the surface prior to anodic film growth. In addition, higher OH^- and lower O^{2-} contents are observed at 30° than at 90°, indicating hydroxides are located primarily in the outer, and oxides in the inner, regions of the film.

The Ni 2p spectra were deconvoluted using the parameter values published by Biesinger et al. [18,19], Fig. 5(b). The relative percentages (Fig. 6(b)) show similar amounts of metallic Ni at −0.4 V and 0 V at both angles, an observation apparently at odds with the signals for Cr and Mo (Fig. 6(c) and (d)) which both decrease over the potential range from −0.4 V to 0 V suggesting passive film thickening. The most likely explanation for this is that, while depleted in the oxide, Ni is slightly enriched in the alloy at the alloy/oxide interface. As expected, the metallic Ni content at 30° is smaller than at 90°. The absence of a signal for metallic Ni at both take-off angles at 0.6 V confirms the presence of a much thicker film at this potential. Comparison of the relative amounts of $Ni(OH)_2$ and NiO measured at the two angles shows a higher $Ni(OH)_2$ content and a lower NiO content at 30° than at 90°, in the passive and transpassive regions, consistent with inner oxide and outer hydroxide regions in the film as indicated by the O 1s spectra.

The Cr 2p spectra were fitted with the parameter values determined by Biesinger [19,20] (Fig. 5(c)), and the relative percentages are shown in Fig. 6(c). The relative percentages of $Cr(OH)_3$ and Cr_2O_3 are much higher and much lower, respectively, at 30° compared to 90°, consistent with an inner Cr_2O_3 barrier layer and outer hydroxide layer. Additionally, unlike for Alloy-22, the Cr_2O_3 content of the film is not significantly decreased at 0.6 V, suggesting the barrier layer may be more durable at 0.6 V in Alloy C-2000 compared to Alloy-22.

The Mo 3d high-resolution scans were fitted with spin–orbit pair intervals set at 3.13 eV and the parameters determined by McIntyre et al. [21] as shown in the example in Fig. 5(d). Mo was found to be present in the film in a range of oxidation states (IV, V, and VI), and the relative percentages are shown in Fig. 6(d). Comparison of the

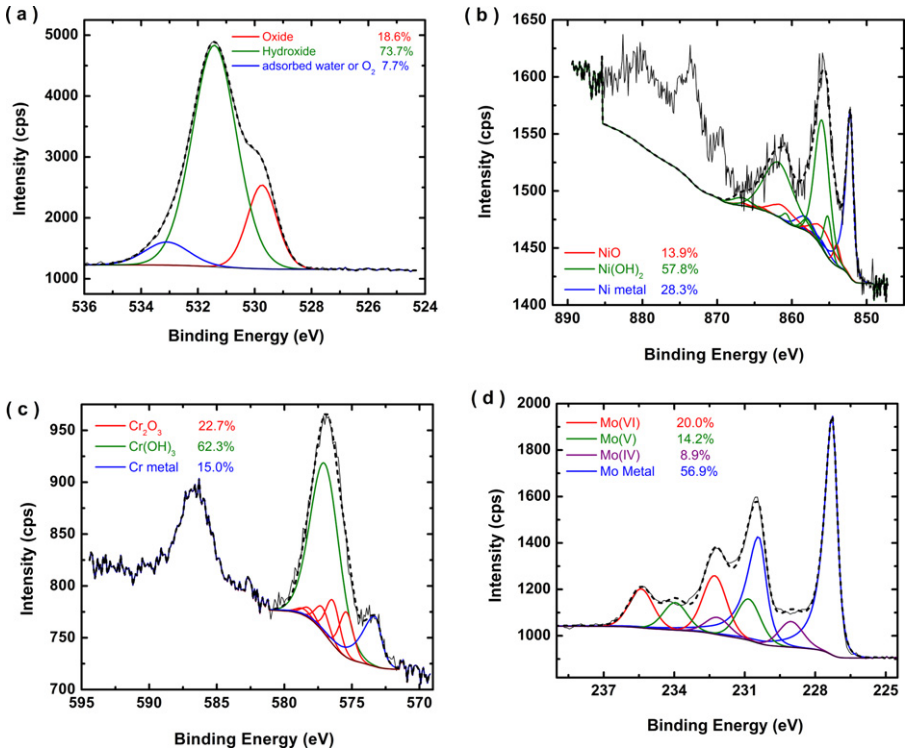

Fig. 5. Examples of high-resolution fitted XPS spectra (a) O 1s (0 V, 90°), (b) Ni 2p (−0.4 V, 30°), (c) Cr 2p (−0.4 V, 30°), and (d) Mo 3d (0 V, 90°) recorded on Alloy C-2000.

relative percentages of Mo species obtained at the two different angles indicates an enrichment of high oxidation states of Mo in the outer region of the film, especially at 0.6 V when the percentage of Mo(VI) increases markedly. Additionally, the percentage of Mo(V) measured at 90° is significantly larger than that at 30° at 0.6 V. In fact, at 30° the percentage of Mo(V) decreases with increasing potential whereas at 90° it increases, indicating a conversion of lower Mo oxidation states in the inner region of the film at 0 V to higher oxidation states in the outer regions of the film at 0.6 V.

A typical Cu $2p_{3/2}$ high-resolution XPS spectrum is shown in Fig. 7. A single peak with a binding energy ranging between 931.8 eV and 932.9 eV was obtained on all specimens. This is close to the

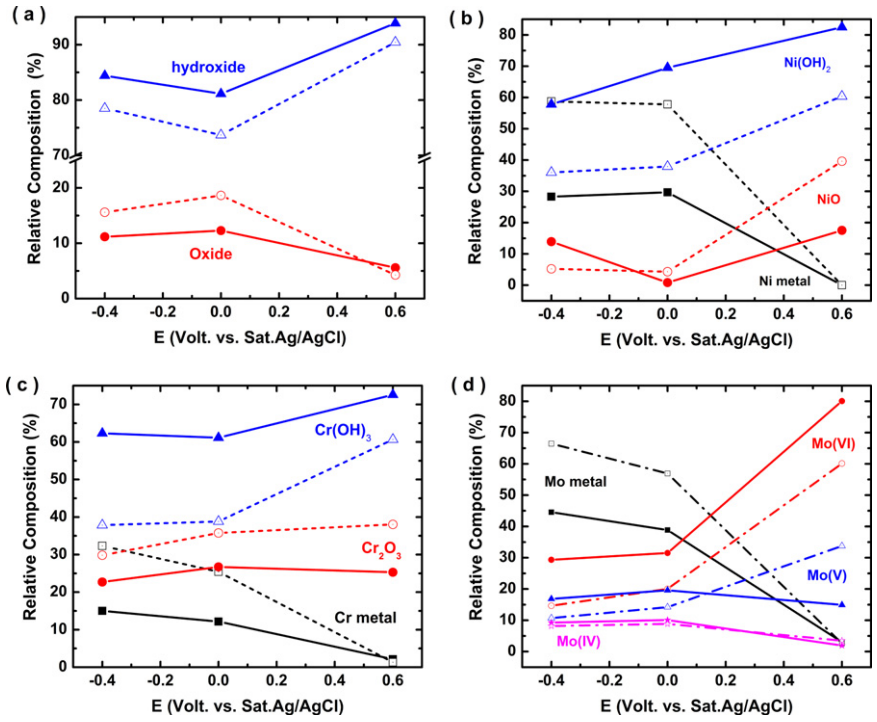

Fig. 6. Relative compositions of O (a), Ni (b), Cr (c), and Mo (d) species in the Alloy C-2000 surface after polarization at −0.4 V, 0 V, and 0.6 V (pH 7, 44 h) at take-off angles of 30° (solid lines) and 90° (dashed lines).

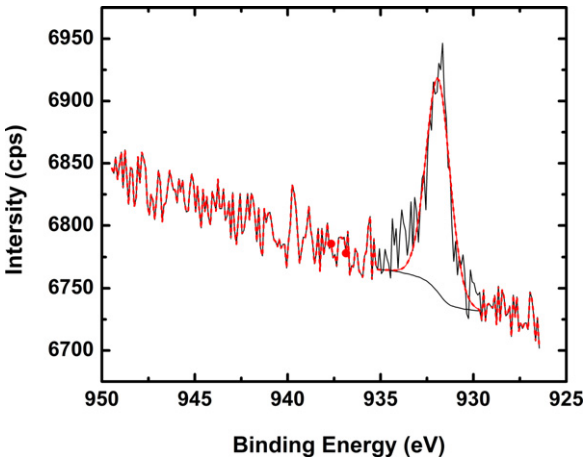

Fig. 7. High-resolution XPS spectrum of Cu $2p_{3/2}$ recorded on Alloy C-2000 after polarization at 0 V (pH 7, 44 h) at a take-off angle of 90°.

binding energy for both Cu metal and cuprous oxide, which are within 0.1 eV of each other and cannot be distinguished by XPS [22]. The well known shake-up satellite peak (5–10 eV higher on the BE scale than the principal Cu $2p_{3/2}$ line), indicative of the presence of the expected Cu(II) species [22–24] at high potentials, was not observed. The absence of Cu(II) species in the film may be due to the decomposition of $Cu(OH)_2$ to Cu(I) under X-ray exposure in the spectrometer [22].

3.4 ToF-SIMS results

ToF-SIMS depth profiles recorded for negative ions after polarization at −0.4 V, 0 V and 0.6 V are shown in Fig. 8. Fig. 9 shows the cross-sectional images for the ions reconstructed from the sputtering profiles. Since the sputtering rate is unknown, conversion of sputtering times cannot be accurately used to calculate film thickness. However, according to Lloyd et al. [1], the passive film thickness on this alloy in acidic solutions (pH 1) is about 2–3 nm. Since the negative ions detected in the ToF-SIMS spectra do not necessarily represent the species which exist in the oxide, the oxidation states of ions cannot be determined. However, in conjunction with other techniques (AR-XPS), ToF-SIMS data can be used to obtain the depth profiles for species within the film.

The sputtering profiles show that each species exhibits a maximum intensity at a specific time, indicating its localization within the film. From the variation in these times, a layered structure of the film can be inferred. Based on peak locations, Cu and Mo oxides segregate to the outer surface of the film, hydroxides of Cr, Ni and Cu are located at intermediate depths, and the inner film region is enriched in Cr and Ni oxides. This layered structure is consistent with the AR-XPS results and is more clearly shown in the cross-sectional images in Fig. 9. It is worth noting that the analytical depth (proportional to sputtering time, Fig. 8) for the surface oxidized at 0.6 V is approximately 6 times larger than that at two lower potentials (as indicated by the arrow labeled "d" in Fig. 9). The much longer sputtering time required at 0.6 V, indicates a significant increase in film thickness as indicated by AR-XPS.

While exact compositions cannot be obtained by this technique, the relative concentrations of various species can be determined if it is assumed that the various oxide components have identical sputtering efficiencies. Fig. 10 shows the $Cr_2O_3^-/MoO_3^-$ (solid line) and $Cr_2O_3^-/CuO^-$ (dotted line) ratios from the sputtering profiles. The increase in the $Cr_2O_3^-/MoO_3^-$ and $Cr_2O_3^-/CuO^-$ ratios from the outer to the inner regions of the film confirms the tendency for the alloy to form a Cr rich inner oxide layer with Mo and Cu segregated to the outer regions. The shorter sputtering time required

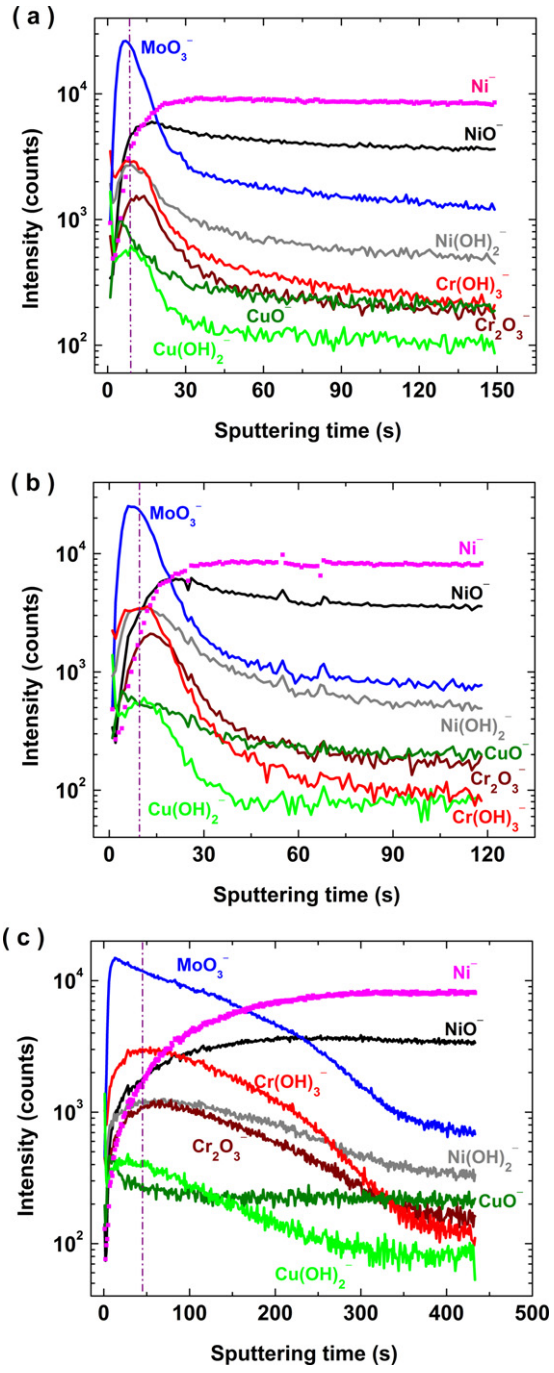

Fig. 8. ToF-SIMS profiles recorded on Alloy C-2000 after polarization at (a) −0.4 V, (b) 0 V and (c) 0.6 V (pH 7, 44 h). The vertical dashed line represents the peak location of $Cr(OH)_3^-$.

to reach a peak in the $Cr_2O_3^-/CuO^-$ ratio, compared to that for $Cr_2O_3^-/MoO_3^-$, indicates a more emphatic surface segregation of Cu than of Mo, consistent with the AR-XPS results and published literature on stainless steels [25] and Fe—Cr alloys [26].

The larger $Cr_2O_3^-/MoO_3^-$ and $Cr_2O_3^-/CuO^-$ ratios obtained on the specimen polarized at 0 V compared to that at −0.4 V, show there is an increase in Cr_2O_3 content of the inner regions of the film with potential, consistent with the development of a barrier layer oxide, as suggested by the AR-XPS results. The lower $Cr_2O_3^-/MoO_3^-$ ratio obtained after polarization at 0.6 V, together with the AR-XPS results, clearly shows the loss of Cr_2O_3 from the film as CrO_4^{2-} [27], and the very broad and shallow peaks in

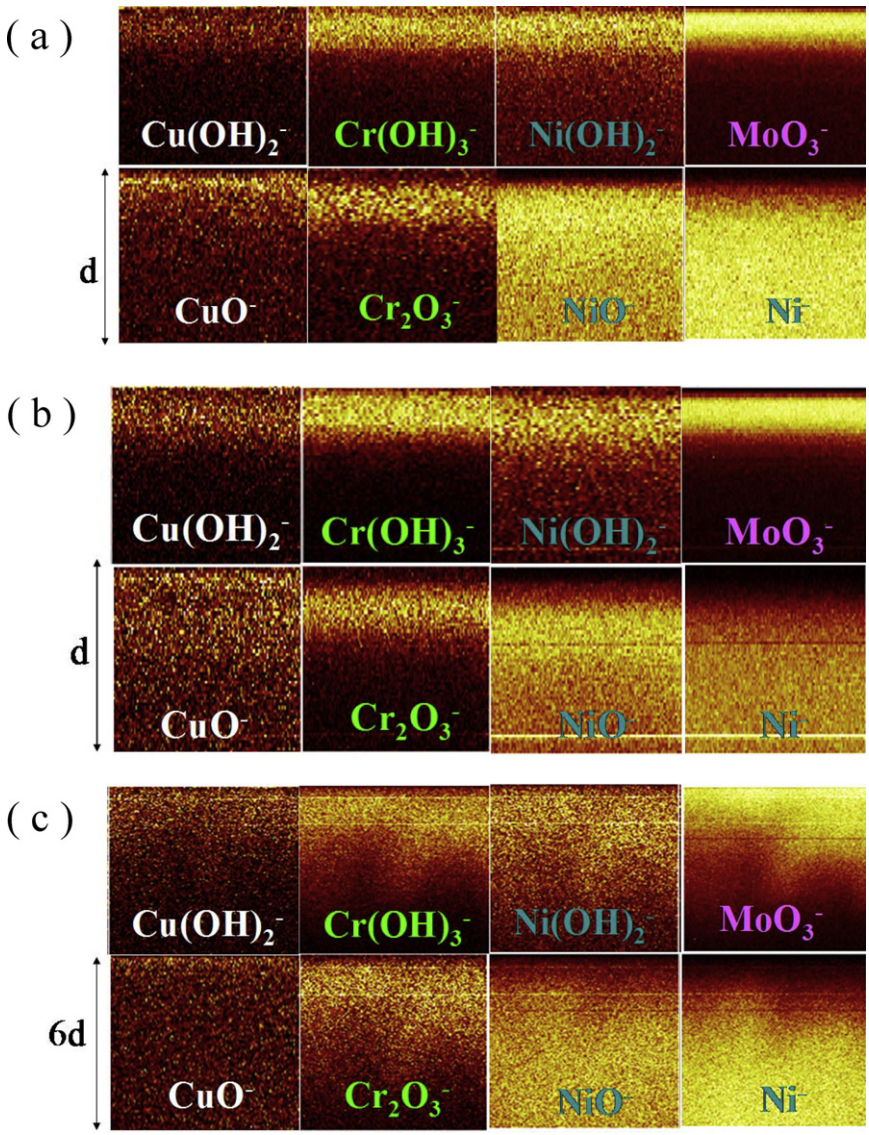

Fig. 9. ToF-SIMS cross-sectional images for Alloy C-2000 reconstructed from sputtering profiles after polarization at (a) −0.4 V, (b) 0 V and (c) 0.6 V (pH 7, 44 h). The lighter colors indicate a higher content of the species shown in the images. (For interpretation of the references to color in this figure legend, the reader is referred to the web version of this article.)

the $Cr_2O_3^-/MoO_3^-$ and $Cr_2O_3^-/CuO^-$ ratios at 0.6 V indicates the destruction of the Cr rich inner layer, leading to a highly defective transpassive oxide [26].

4. Discussion

As previously observed for Alloy-22, the oxide film on Alloy C-2000 exhibits a bilayer structure consisting of a Ni/Mo-containing inner Cr(III) oxide barrier layer formed directly on the alloy surface and an outer hydrous oxide layer formed by hydrolysis of cations ejected from the barrier layer. This separation between an oxide-dominated inner layer and an outer hydroxide-dominated layer is clearly demonstrated by AR-XPS.

As the applied potential is increased from −0.4 V (near passive region) to 0 V (passive region) the XPS results indicate an increase in film thickness accompanied by an increase in Cr(III) content of the inner oxide, consistent with previous observations for Alloy-22 [1,2,8,13]. The observation that the relative Cr content of the film increases while that of Ni decreases with potential leading to an increased Cr content of the inner oxide indicates the principle process leading to passivity is the dissolution of Ni and retention of Cr, in agreement with previous observations by Lloyd et al. in acidic sulphate solutions [2].

This improved passivity with increasing Cr(III) oxide content was demonstrated for Alloy-22 by EIS measurements [6] and confirmed for C-2000 in a similar manner [to be published]. It is worth noting that the Cr(III) oxide content of the inner layer for Alloy C-2000 in this study (>30%) is considerably higher than that obtained after anodic polarization of Alloy-22 (≤10%). This difference most likely reflects the longer duration of anodic oxidation in the present case (44 h) compared to the Alloy-22 study (2 h) rather than the influence of any specific differences in composition (the absence of W (3 wt.% in Alloy-22) and the presence of Cu (1.6 wt.% in C-2000)) although this remains to be unequivocally demonstrated [28].

The Cr/Mo segregation process, observed primarily by ToF-SIMS, has been previously observed for Mo-containing stainless steels [29] and Ni—Cr—Mo alloys [1–3]. It has been claimed that the Mo(VI) in the outer layer of the oxide is stabilized as MoO_4^{2-} by the high electric field leading to deprotonation of OH^- within the film which supplies O^{2-} to enhance the formation of the Cr(III) inner oxide [30].

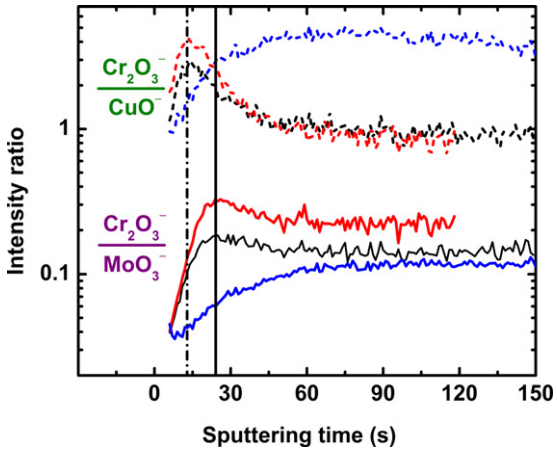

Fig. 10. $Cr_2O_3^-/MoO_3^-$ (solid line) and $Cr_2O_3^-/CuO^-$ (dotted line) intensity ratios from ToF-SIMS sputtering profiles recorded on Alloy C-2000 after polarization at −0.4 V (black), 0 V (red) and 0.6 V (blue) (pH 7, 44 h). The vertical dashed and solid lines represent the locations of the peak $Cr_2O_3^-/CuO^-$ and $Cr_2O_3^-/MoO_3^-$ ratios, respectively. (For interpretation of the references to color in this figure legend, the reader is referred to the web version of this article.)

The accumulation of a Cu layer on the surface of Ni—Cr—Mo alloys has not been observed previously. On 304 stainless steel containing 0.19 wt.% Cu, Ogle et al. [31] used linear sweep voltammetry coupled to downstream atomic emission spectroelectrochemistry (AESEC) to show congruent dissolution of Fe, Cr, Ni, Mn and Mo but delayed release of Cu. EDX analysis of the surface layer on 304 stainless steel (1.9 wt.% Cu) showed an increase in Cu content to 6.91 wt.% confirming its retention on the steel surface [32]. The overall suppression of anodic dissolution was attributed to the accumulation of this layer [32]. Itzhak and Peled [33] claimed that the deposition of Cu on the surface of 316 sintered stainless steel containing 0.25–5.0 wt.% Cu improved the corrosion resistance. Seo et al. [34] found that Cu suppressed the anodic dissolution of Fe—26Cr in 1 M H_2SO_4. The morphology of the deposited Cu was found to vary on the surfaces of ferritic and austenitic steel [35], but a metallic Cu layer was found by most workers [32].

The beneficial effect of alloying with Cu has been attributed to the stability of deposited Cu on an anodically oxidized surface [36], but also to the presence of Cu in solid solution and Cu-rich phases in the matrix of the alloy, and to the rapid formation of a Cu-rich surface layer during active dissolution [37].

However, Seo et al. [34] claimed that Cu reduces the stability of the passive layer, and also the passive film on Cu-bearing stainless steels was destroyed by Cl^- attack more easily than that on steel containing no Cu [35]. Lizovs [38] found that Cu reduces the stability of the passive layer on stainless steels containing less than 1% Mo, but this reduction was over-ridden when the Mo content was increased to 3%. In addition, the suppression of anodic dissolution by the deposited Cu was only observed in the potential range in which it was stable. At more positive potentials, Cu dissolved as $CuCl_2^-$ in solutions of low pH and high Cl^- concentrations, and the dissolution potential shifted in an active direction as the Cl^- concentration was increased [31,35]. It was also suggested that the dissolution of Cu as complexes $CuCl^-$, $CuCl_4^{2-}$, $CuCl_2^-$ and $CuCl_3^{2-}$ might assist the destruction of the passive film, making Cu harmful to the localized corrosion resistance of both ferritic and austenitic stainless steels [35]. The details of the effect of alloying with Cu remain uncertain.

The enrichment of Cu in the outer region of the oxide film on Alloy C-2000 is consistent with the results for stainless steels. However, the chemical state of the Cu is difficult to determine by XPS and ToF-SIMS techniques, due to the possibility of the reduction of Cu(II) species to Cu(I) under X-ray exposure [22]. Also, the closeness of the BE for Cu metal and cuprous oxide, makes their separation in XPS spectra extremely difficult. Based on thermodynamic evidence [35,39], metallic Cu would be expected on the surface of Alloy C-2000 at −0.4 V, while at 0 V and 0.6 V, Cu^+ and Cu^{2+} would be the stable forms, respectively. The CuO and $Cu(OH)_2$ found in the surface of Alloy C-2000 by ToF-SIMS sputtering profiles and images may be due to the ion interactions in the sputtering/analysis chamber in the instrument, and cannot be used to confirm the oxidation state of the Cu. However, the SEM images show no evidence for the separation of any crystalline forms on the surface of the alloy in the passive (0 V) and transpassive (0.6 V) regions. This could suggest that the Cu is incorporated in the outer regions of the film in the Cu(I) and/or Cu(II) states, although the present analyses could not confirm this.

The composition and structure of the passive film change considerably when the film-growth potential is extended into the transpassive region (0.6 V). A much thicker but non-uniformly distributed film was observed. The transpassive oxidation of Cr(III) to Cr(VI) in the barrier layer of the film and its subsequent dissolution, leads to the destruction of the Cr_2O_3-enriched inner layer, as indicated by the extremely low relative oxide to hydroxide content in the AR-XPS results, and the loss of a peak in the $Cr_2O_3^-/MoO_3^-$ intensity ratio obtained from ToF-SIMS sputtering profiles. The oxidative dissolution of Cr(III) leads to the introduction of a large number of cation vacancies in the film and a decrease in polarization resistance [6,8]. This destruction of passivity allows the transport of Ni through the film and its dissolution at the oxide/solution interface. Also, the percentage of Mo(VI) increases markedly, indicating a conversion of lower Mo oxidation states in the inner regions of the passive film to higher oxidation states in the outer regions. Additionally, the AR-XPS data shows oxidation of Mo(IV) to higher oxidation states takes place in the inner layer of the film.

The SEM evidence in Fig. 2 suggests this accumulation retards extensive dissolution. Although the XPS results (Fig. 6(c)) suggest the Cr(III) oxide content of the barrier layer is high at this potential it does not prevent the onset of transpassive behavior. This apparent contradiction may reflect the local nature of the onset of transpassivity (Fig. 2) with areas of intact passive film coexisting with transpassively degraded areas.

5. Summary and conclusions

The passive and transpassive properties of oxide films on C-2000 at various potentials were investigated by AR-XPS, ToF-SIMS and SEM. The presence of a layered structure in the passive film has been demonstrated, with the outermost surface being enriched in Cu (or Cu oxide) and Mo oxide, the intermediate region dominated by Cr/Ni hydroxides, and the inner region comprising Cr/Ni oxide.

As the film growth potential is increased into the transpassive region (0.6 V) the oxidative destruction of the Cr(III)-dominated barrier layer occurs non-uniformly on the surface of the alloy. This may account for the AR-XPS observation that the Cr_2O_3 content of the surface layer does not apparently decrease and indicates that transpassive oxidation tends to spread laterally across the surface and the higher oxidation states of Mo produced transpassively, and shown to accumulate by ToF-SIMS, form a partially protective film. This film is approximately six times thicker than the passive film present at less positive potentials.

As potential increases from −0.4 to 0.6 V, the film thickness increases, and the relative Cr content of the film increases while that of Ni decreases. The passive film (0 V) has a relatively thicker inner oxide layer and higher Cr_2O_3 content in the inner layer, compared to the near-passive film (−0.4 V). When the film-growth potential is extended into the transpassive region (0.6 V), the composition and structure of the film change considerably. The transpassive

oxidation of Cr(III) to Cr(VI) in the barrier layer of the film and its subsequent dissolution leads to the loss of the Cr_2O_3-rich inner layer and the destruction of passivity.

Acknowledgements

The authors gratefully acknowledge the U.S. Department of Energy and the National Science and Engineering Research Council of Canada (NSERC) for the funding sources, and Haynes International, Kokomo, Indiana, for their generous donation of materials. Special thanks go to Dr. Mark Biesinger, Dr. Heng-Yong Nie, and Mr. Ross Davidson at Surface Science Western (SSW), for their knowledge and assistance on the analytical techniques employed in this study.

References

[1] A.C. Lloyd, D.W. Shoesmith, N.S. McIntyre, J.J. Noël, Effect of temperature and potential on the passive corrosion properties of alloys C 22 and C 276, Journal of the Electrochemical Society 150 (2003) B120.
[2] A.C. Lloyd, J.J. Noël, S. McIntyre, D.W. Shoesmith, Cr, Mo and W alloying additions in Ni and their effect on passivity, Electrochimica Acta 49 (2004) 3015.
[3] A.C. Lloyd, J.J. Noël, N.S. McIntyre, D.W. Shoesmith, The open-circuit ennoblement of alloy C-22 and other Ni-Cr-Mo alloys, Journal of the Minerals, Metals and Materials Society 57 (2005) 31.
[4] J.J. Gray, B.S. El Dasher, C.A. Orme, Competitive effects of metal dissolution and passivation modulated by surface structure: an afm and ebsd study of the corrosion of alloy 22, Surface Science 600 (2006) 2488.
[5] J. Hayes, A.W. Szmodis, K. Anderson, C.A. Orme, Effect of the Environment and Alloy Composition on the Electrochemical Behavior of Ni-Cr-Mo Alloys. Corrosion, Paper No. 04697, NACE, New Orleans, LA, March 28–April 1, 2004.
[6] P. Jakupi, D. Zagidulin, J.J. Noël, D.W. Shoesmith, The impedance properties of the oxide film on the Ni-Cr-Mo Alloy-22 in neutral concentrated sodium chloride solution, Electrochimica Acta 56 (2011) 6251.
[7] D.D. Macdonald, A. Sun, An electrochemical impedance spectroscopic study of the passive state on alloy 22, Electrochimica Acta 51 (2006) 1767.
[8] N. Priyantha, P. Jayaweera, D.D. Macdonald, A. Sun, An electrochemical impedance study of alloy 22 in Nacl brine at elevated temperature. I. Corrosion behavior, Journal of Electroanalytical Chemistry 572 (2004) 409.
[9] M. Bojinov, P. Kinnunen, G. Sundholm, Electrochemical behavior of Nickel-Chromium alloys in a high-temperature aqueous electrolyte, Corrosion 59 (2003) 91.
[10] M. Bojinov, A. Galtayries, P. Kinnunen, A. Machet, P. Marcus, Estimation of the parameters of oxide film growth on nickle-based alloys in high-temperature water electrolytes, Electrochimica Acta 52 (2007) 7475.
[11] P. Jakupi, J.J. Noël, D.W. Shoesmith, Intergranular corrosion resistance of sigma 3 grain boundaries in Alloy 22, Electrochemical and Solid-State Letters 13 (2010) C1.
[12] P. Jakupi, F. Wang, J.J. Noël, D.W. Shoesmith, Corrosion product analysis on crevice corroded alloy-22 specimens, Corrosion Science 53 (2011) 1670.
[13] D. Zagidulin, X. Zhang, J. Zhou, J.J. Noël, D.W. Shoesmith, Characterization of surface composition on alloy-22 in neutral chloride solutions, Surface and Interface Analysis, submitted for publication.
[14] D.D. MacDonald, A. Sun, N. Priyantha, P. Jayaweera, An electrochemical impedance study of alloy-22 in Nacl brine at elevated temperature: ii. Reaction mechanism analysis, Journal of Electroanalytical Chemistry 572 (2004) 421.
[15] R.S. Lillard, M.P. Jurinski, J.R. Scully, Crevice corrosion of alloy 625 in chlorinated astm artificial ocean water, Corrosion 50 (1994) 251.
[16] B.A. Kehler, G.O. Ilevbare, J.R. Scully, Crevice corrosion stabilization and repassivation behavior of Alloy 625 and Alloy 22, Corrosion 57 (2001) 1042.
[17] B.A. Kehler, G.O. Ilevbare, J.R. Scully, Crevice corrosion stabilization and repassivation behavior of Alloy 625 and Alloy 22, corrosion (Houston, TX, United States), Corrosion 61 (2005) 665.
[18] M.C. Biesinger, B.P. Payne, L.W.M. Lau, A. Gerson, R.S.C. Smart, X-Ray photoelectron spectroscopic chemical state quantification of mixed nickel metal, oxide and hydroxide systems, Surface and Interface Analysis 41 (2009) 324.
[19] M.C. Biesinger, B.P. Payne, A.P. Grosvenor, L.W.M. Lau, A.R. Gerson, R.S.C. Smart, Resolving surface chemical states in Xps analysis of first row transition metals, oxides and hydroxides: Cr, Mn, Fe, Co and Ni, Applied Surface Science 257 (2011) 2717.
[20] M.C. Biesinger, C. Brown, J.R. Mycroft, R.D. Davidson, N.S. McIntyre, X-Ray photoelectron spectroscopy studies of chromium compounds, Surface and Interface Analysis 36 (2004) 1550.
[21] P.A. Spevack, N.S. McIntyre, Thermal reduction of Moo3, Journal of Physical Chemistry 96 (1992) 9029.
[22] N.S. McIntyre, S. Sunder, D.W. Shoesmith, F.W. Stanchell, Chemical Information from Xps – applications to the analysis of electrode surfaces, Journal of Vacuum Science & Technology 18 (1981) 714.
[23] B. Wallbank, C.E. Johnson, I.G. Man, Surface reduction of solid 3d transition-metal compounds during X-ray photoelectron-spectroscopy, Journal of Electron Spectroscopy and Related Phenomena 4 (1974) 263.
[24] S. Poulston, P.M. Parlett, P. Stone, M. Bowker, Surface oxidation and reduction of Cuo and Cu2o studied using Xps and Xaes, Surface and Interface Analysis 24 (1996) 811.
[25] C.R. Clayton, I. Olefjord, Passivity of Austenitic Stainless Steels, in: P. Marcus (Ed.), Corrosion Mechanisms in Theory and Practice, third edition, CRC Press, New York, 2012, p. 327, Chapter 6.
[26] M. Bojinov, G. Fabricius, T. Laitinen, K. Mäkelä, T. Saario, G. Sundholm, Influence of molybdenum on the conduction mechanism in passive films on iron-chromium alloys in sulphuric acid solution, Electrochimica Acta 46 (2001) 1339.
[27] D.S. Dunn, C.S. Brossia, O. Pensado, long-term dissolution behavior of Alloy 22: Experiments and Modeling, Corrosion 2001 NACE International, March 26-31 (2001).
[28] A. Schneider, D. Kuron, S. Hoffman, R. Kirchheim, Aes analysis of pits and passive films formed on Fe-Cr Fe-Mo and Fe-Cr-Mo alloys, Corrosion Science 31 (1990) 191.
[29] C.R. Clayton, Y.C. Lu, A bipolar model of the passivity of stainless steel: the role of mo addition, Journal of Electrochemical Society 133 (1986) 2465.
[30] K. Ogle, J. Baeyens, J. Swiatowska, P. Volovitch, atomic emission spectroelectrochemistry applied to dealloying phenomena: I. The formation and dissolution of residual copper films on stainless steel, Electrochimica Acta 54 (2009) 5163.
[31] M. Asawa, A. Devasenapathi, M. Fujisawa, Effect of corrosion product layer on scc susceptibility of copper containing type 304 stainless steel in 1 M H2so4, Materials Science and Engineering a-Structural Materials Properties Microstructure and Processing A366 (2004) 292.
[32] D. Itzhak, P. Peled, The effect of Cu addition on the corrosion behavior of sintered stainless-steel in H2so4 environment, Corrosion Science 26 (1986) 49.
[33] M. Seo, G. Hultquist, C. Leygraf, N. Sato, The Influence of minor alloying elements (Nb, Ti and Cu) on the corrosion resistivity of ferritic stainless-steel in sulfuric-acid-solution, Corrosion Science 26 (1986) 949.
[34] T. Ujiro, S. Satoh, R.W. Staehle, W.H. Smyrl, Effect of alloying cu on the corrosion resistance of stainless steels in chloride media, Corrosion Science 43 (2001) 2185.
[35] A. Pardo, M.C. Merino, M. Carboneras, F. Viejo, R. Arrabal, J. Munoz, Influence of Cu and Sn content in the corrosion of Aisi 304 and 316 stainless steels in H2so4, Corrosion Science 48 (2006) 1075.
[36] A.A. Hermas, K. Ogura, T. Adachi, Accumulation of copper layer on a surface in the anodic polarization of stainless-steel containing cu at different temperatures, Electrochimica Acta 40 (1995) 837.
[37] E.A. Lizovs, Effects of Mo, Cu, Si and P on anodic behavior of 17 Cr steels corrosion (Houston, TX, United States), Corrosion 22 (1966) 297.
[38] N.S. McIntyre, S. Sunder, D.W. Shoesmith, F.W. Stanchell, J. Vac. Sci. Technol 18 (1981) 714.
[39] M. Pourbaix, Atlas of Electrochemical Equilibria in Aqueous Solutions, Pergamon Press, Cebelcor, Brussels, 1966.